Planar and SPECT Monte Carlo acceleration using a variance reduction technique in I[131] imaging

H.R. Khosravi[1, 2*], S. Sarkar[1, 3], A. Takavar[1, 4], M. Saghari[4], M. Shahriari[5]

[1] Department of Medical Physics, Faculty of Medicine, Tehran University of Medical Sciences, Tehran, Iran
[2] National Radiation Protection Department, Iranian Nuclear Regulatory Authority, Tehran, Iran
[3] Research Center for Science and Technology in Medicine, Tehran University of Medical Sciences, Tehran, Iran
[4] Department of Nuclear Medicine, Shariati Hospital, Tehran University of Medical Sciences, Tehran, Iran
[5] Department of Medical Radiation, Shahid Beheshti University, Tehran, Iran

Background: Various variance reduction techniques such as forced detection (FD) have been implemented in Monte Carlo (MC) simulation of nuclear medicine in an effort to decrease the simulation time while keeping accuracy. However most of these techniques still result in very long MC simulation times for being implemented into routine use. ***Materials and Methods:*** Convolution-based forced detection (CFD) method as a variance reduction technique was implemented into the well known SIMIND MC photon simulation software. A variety of simulations including point and extended sources in uniform and non-uniform attenuation media, were performed to compare differences between FD and CFD versions of SIMIND modeling for I[131] radionuclide and camera configurations. Experimental measurement of system response function was compared to FD and CFD simulation data. ***Results:*** Different simulations using the CFD method agree very well with experimental measurements as well as FD version. CFD simulations of system response function and larger sources in uniform and non-uniform attenuated phantoms also agree well with FD version of SIMIND. ***Conclusion:*** CFD has been modeled into the SIMIND MC program and validated. With the current implementation of CFD, simulation times were approximately 10-15 times shorter with similar accuracy and image quality compared with FD MC. **Iran. J. Radiat. Res., 2007; 4 (4): 175-182**

Keywords: *Monte Carlo, convolution forced detection, SPECT, SIMIND, nuclear medicine.*

INTRODUCTION

Monte Carlo (MC) program is a well-known technique to simulate photon traveling, energy and hardware simulation for different purposes. It is a well used method in nuclear medicine research and clinical practice. During MC simulation, random numbers are sampled to model photon activity and to calculate photon probability at every location with the object or gamma camera (figure 1A). There are two main MC codes: first, standard or general-purpose MC program i.e. MCNP, GEANT4 and EGS4; second, dedicated MC program for nuclear medicine applications namely SIMIND [(1)], SimSET [(2)] and Geant4 application for tomographic Emission (GATE) [(3)].

These codes are effective tools to perform accurate problem modeling in planar and SPECT imaging, but suffer from long computation time especially standard ones. As a result, a number of variance reduction techniques (VRT) have been introduced to accelerate the MC [(4)]. Dedicated MC program like SIMIND track photon in the object, and project it onto detector at only a randomly sampled detector location. In fact they use FD [(5, 6)] technique which is convolution of photon probability with a δ function.

In CFD method, FD is used and combined with convolution-based modeling of collimator response and intrinsic camera resolution [(7, 8)].

Creating almost noise-free projections are desirable in model-based iterative reconstruction, in order to minimize the noise-level in the reconstructed images. Unfortunately, it still takes much time to obtain these kinds of projections with MC,

*Corresponding author:
Hamid Reza Khosravi, Department of Medical Physics,
Tehran University of Medical Sciences, Tehran, Iran.
Fax: *+98 21 66439833*
E-mail: *hrkhosravi@razi.tums.ac.ir*

despite the use of known VRTs like FD. Therefore, it is very important to further reduce the time needed to generate almost noise-free projections.

This is especially true for high energy photon radionuclide such as I^{131} which has complicated radiation decay and requires the modeling of back scattering off camera components behind the crystal and the penetration of the walls of the collimator.

The aim of this work is to implement further improvements to MC modeling in order to provide faster and more accurate simulations of planar and SPECT I^{131} imaging by implementing CFD into SIMIND MC dedicated program.

MATERIALS AND METHODS

CFD modeling

In regular SIMIND, the path of a photon through an object is evaluated and considered as photoelectric absorption and Compton scattering. When a photon reached the last scatter point in the simulated object, it is projected into a single location on the gamma camera. To do this, SIMIND uses the FD process whereby at the last point of scatter within the object, the photon is always directed towards the gamma camera. The location projected to the camera is a random location within the collimator response function. As such, the detected location is something like what you can see in figure 1A.

In CFD method, regular SIMIND is used to track the transit of photons through the object, and again the last scatter point is used to project the photon onto an area of gamma camera. Indeed, by calculating analytical point spread function (PSF), photon gets blurred over this area on detector. However, rather than projecting the photon to a single point within the collimator response function, the photon is projected into all points within the response function. This is typically Gaussian shaped, and varies with source-detector or (collimator) distance, intrinsic resolution and collimator type (figure 1B).

A blurring kernel defined by the PSF is implemented analytically to model detector response based on collimator parameters and source-detector distance. The positions and weights of last photon scatter site (x,y,z) are stored in a sub-projection layer during photon transport (figure 1C). And this sub-projection layer is convolved with an appropriate PSF.

In the case of septal penetration, the blurring kernel is calculated according to new collimator subroutine that includes collimator interaction (scatter and penetration) as well as geometric response function [9].

CFD is inserted into SIMIND MC Version 4.4 code in order to improve simulation time and accuracy. Implementation of CFD into SIMIND was performed by using a FORTRAN script routine named "score.f" which SIMIND author has provided the opportunity for user to make its own code implementing. These routines should set up the different energy windows used for acquisition of photons and therefore are
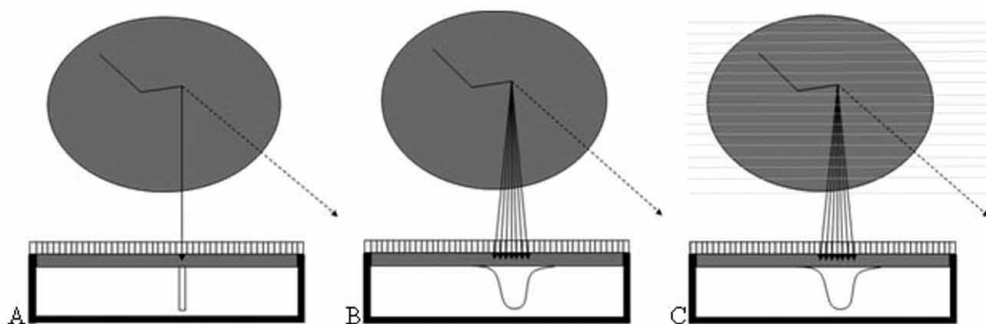
Figure 1. Illustration of different scatter photon simulation, A) FD detection, B) CFD detection and C) showing the layers for CFD detection.

isotope specific and uses their own photon energies and probabilities. At various steps during the photon transit process, SIMIND looks to the score.f routine to see what it should do. If there was a score.f it execute the script, otherwise the normal SIMIND will run. It should be noted that we use our own source and density maps as input files to SIMIND for all experiments and it didn't use any SIMIND internal source or density map and isotope specifications.

Simulation

Different projections of I¹³¹ point and block sources in air and extended emission distributions in the voxelised Zubal phantom [10] were generated.

The simulations included 3 orders of scatter. Projections were simulated with the camera position exactly such as SIMIND coordinate system. The collimator parameters used was high energy general purpose parallel-hole for GE-Infinia (*GE Healthcare-Americas, Milwaukee, WI, USA*) and ADAC Epic Argus (ADAC Laboratories, 540 Alder Drive, Milpitas, CA 95035, USA) gamma cameras. Hole shapes of collimators were hexagonal.

To simulate the photons that re-enter the NaI crystal after backscattering off various objects behind the crystal, in this work a 5cm slab of Pyrex was used directly below the NaI crystal to include the effect of backscattered photons [11].

The energy resolution was set to ±10%, the energy windows were centered at 364 keV. The voxel sizes were 0.442cm×0.442cm×0.442cm for 3D Zubal phantom with a 128×128×128 matrix size and 0.221cm×0.221cm×0.221cm with a grid sizes of 256×256×256 for point, sheet and block sources.

For Zubal phantom, the relative activity concentrations were chosen as the background, the lungs, the kidneys, the liver, the myocardium and the lesions in the ratio 1:5:50:50:100:250, respectively. Images were generated in 128×128 transaxial and 1 axial projection using a 0.442 cm projection bin size. The photon history to create low-noise MC projections was 2×10^9 [7] that there were

8.7×10^8 average counts in each pixel.

Evaluation of MC method

In order to evaluate CFD code the following works have been done. Projections were experimentally measured and simulated for I¹³¹ point sources to measure system PSF. And also point and extended sources in uniform and non-uniform (Zubal) phantoms [10] were simulated with both regular FD and CFD SIMIND.

First of all, the system point spread function (PSF) was measured using a ~1 mm diameter point source (196 MBq for I¹³¹) in air at different distances. Then, the results were compared with the results from FD and CFD simulation of a point source in air at 0-50 cm with 5 cm interval distances. The point source was positioned so that it was approximately directly over the centre of a collimator hole and was moved along the direction parallel to the holes' axis to different distances from the collimator face. The projection images were recorded into 1024×1024 matrices with a 0.5525 mm pixel size. The same parameters were used in the FD and CFD simulation.

The system point spread function was calculated by fitting profiles of the point source projection images with a Gaussian function (this performs in accordance with NEMA specifications in terms of fit parabolic function to peak with linear interpolation). The system point spread function in pixels was then multiplied by the pixel size (0.05525 cm) to yield the system PSF (FWHM) in cm.

The photon history to create low-noise MC projections for point sources was 15×10^8 [7] that there were 4.45×10^8 average counts in each pixel.

Validation methods

The accuracy of CFD was validated by the following method:
1) Point source response based on comparison between experiment, FD and CFD according to section 2.3.

The correlation coefficient was calculated between FD-experimental data and CFD-experimental data according to the question 1:

$$r^2 = \frac{(\Sigma xy - n\overline{xy})^2}{(\Sigma x^2 - n\overline{x}^2)^2(\Sigma y^2 - n\overline{y}^2)^2} \qquad (1)$$

where r^2 (R-square) is the square of the correlation between the experimental data and the simulated data values, each r^2 value closer to 1 indicating a better fit. x, $\overline{x}$ are experimental data and its mean, y, $\overline{y}$ are FD or CFD data and their mean, n is the number of data points.

2) Simulation times of sheet and block source projections for a given noise level. The coefficients of variation were calculated as ratio between standard deviation and mean pixel value of projections and their simulation times.

3) FD and CFD projections of Zubal phantom for different histories compared to low noise projection generated by FD method. The high count standard FD projection is referred to as reference projection. Also, the noise and error properties of CFD and FD estimated projections were compared by taking the Universal Image Quality Index (UIQI) [12] in the estimated projections using the reference projection

To compare reference projections to CFD and FD projections, UIQI method includes and considers correlation coefficient, luminance and contrast between reference and estimated projections. UIQI values or in short term Q values closer to 1 indicate a better match to reference projection image. The speed-up factor of CFD was determined by comparing the simulation times of CFD and FD estimated projections at equal CV for uniform sources and Q factor for non-uniform phantoms.

RESULTS

Figure 2 shows the acquired and simulated spatial resolution results in terms of FWHM for a point source of I^{131} in air along both X (A) and Y (B) axes for the GE-Infinia camera with HEGP collimator, respectively.

A very good agreement between experiments, FD and CFD simulations can be seen for both axes and or both codes. Some small

differences were seen which are likely due to the inaccuracy in the alignment of the point source to the axis of the collimator holes and /or are probably related to inaccuracies in the measurement of the energy resolution or the assumption that it depends on the square root of energy or misalignment of the photopeak with the energy-window centre.

It has to be mentioned that due to the influence of collimator septa, the resulting profiles can exhibit fluctuations which are

A

B
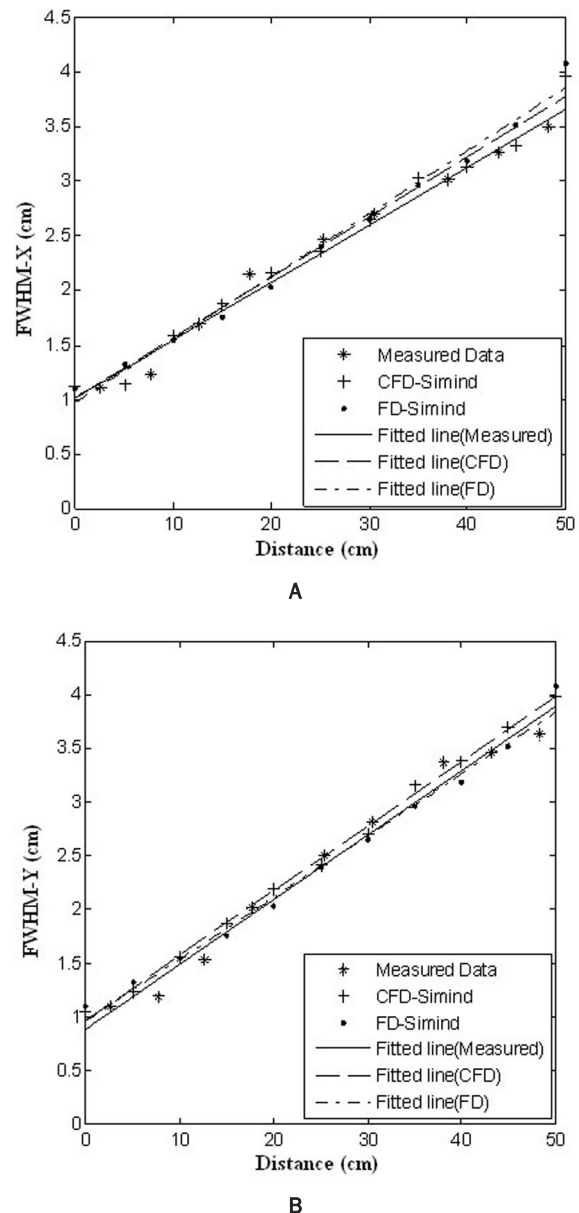
Figure 2. Comparison of the spatial resolutions, measured, FD and CFD simulated for I^{131}
A: X-direction B: Y-direction for (GE-Infinia Camera).

difficult to be fitted to a Gaussian function, and that is normal in the case of using septal penetration mode in MC simulations as well as experimental data.
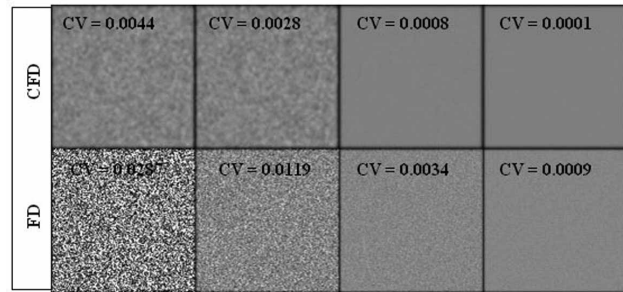
The above value in each cell of table 1 shows the slopes and intercepts of fitted lines to each set of PSF data (experiments and FD & CFD simulations) that represents the values for PSF as a function of the distance between the point source and the collimator face. The values in the second row of each cell in table 1 show the R-square (correlation coefficient) values of FD and CFD simulations that represents the high accuracy of FD and CFD simulations against experimental data ($r^2 > 0.97$). The system PSF exhibits a linear behavior, in either directions (X & Y), which can be considered as good criteria to validate CFD code which is in agreement with the results obtained by other researchers [13, 14].

Figure 3. Sample comparisons of quality and CV values for I^{131} sheet source with 0.65, 6.5, 65, 655 million histories from left to right, respectively. The CV values have been written for each projection.

and FD. The computation time of CFD-MC is much less than FD-MC for the same CV value. In order to get to the same CV values, it takes 10 times less with CFD in comparison with FD method.

Table 1. System Point Spread Functions for GE-Infinia camera for I^{131} with HEGP collimator.

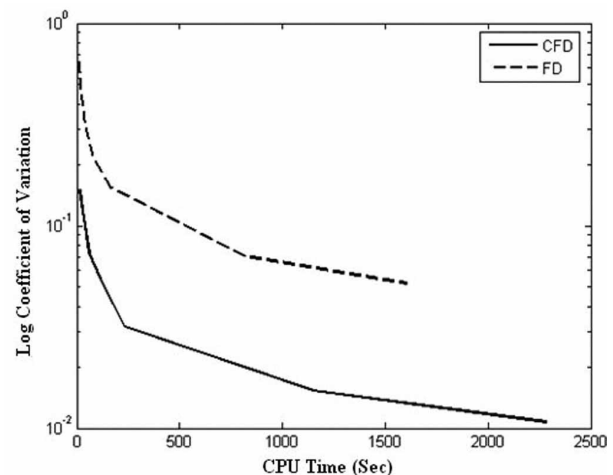|	FWHM-X (cm)	FWHM-Y (cm)
Experiment	0.0530x+1.0160	0.0603x+0.8869
FD SIMIND	0.0577x+0.9743 ($r^2 = 0.9809$)	0.0576x+0.9621 ($r^2 = 0.9817$)
CFD SIMIND	0.055x+1.0130 ($r^2 = 0.9924$)	0.0621x+0.9642 ($r^2 = 0.9763$)

Figure 3 shows the sample projections of I131 sheet source for CFD and FD MC (top and below rows, respectively) with 0.65, 6.5, 65, 655 million histories from left to right, respectively. The projection images were acquired in a 256×256 matrix with a 0.221 cm pixel sizes. The CV values have been indicated for each projection. As one can see on the figure, the CV values of CFD-SIMIND for the same photon histories are less than FD-SIMIND and the excellent uniformity of CFD images can be easily seen.

As seen in figure 4, the CV against CPU time in a semi-logarithmic scale for uniform cubic block sources for I^{131}. In this study projection images of a cubic phantom filled with I^{131} has been simulated using both CFD

Figure 4. log CV vs CPU time in block source using FD (dashed line) and CFD (solid line) for I131 isotope.

Simulated projections of the extended emission distribution in the Zubal phantom are shown in figure 5. The estimated projections are based on 8×10^7 photon histories generated using CFD and FD. Figure 5B shows CFD projection of Zubal phantom, and figure 5C shows FD projection of the same phantom. As a reference, a projection based on standard FD and 2×10^9 photon histories is included in top row.

It is clearly visible that for equivalent numbers of simulated photon histories, the estimated projections generated with CFD are less noisy than estimated projections
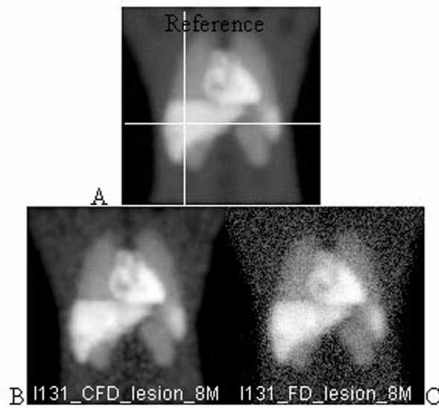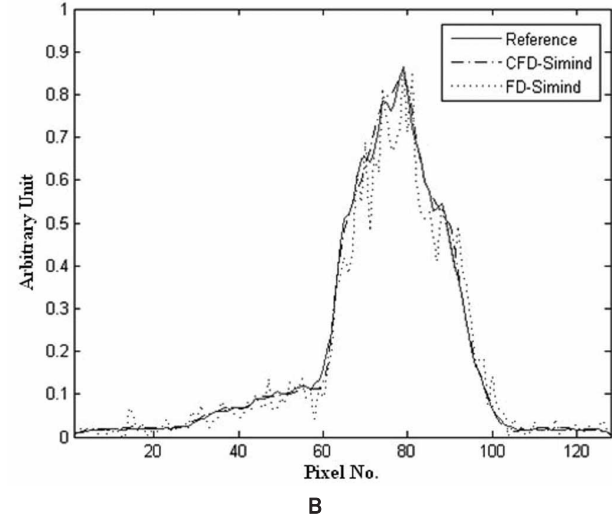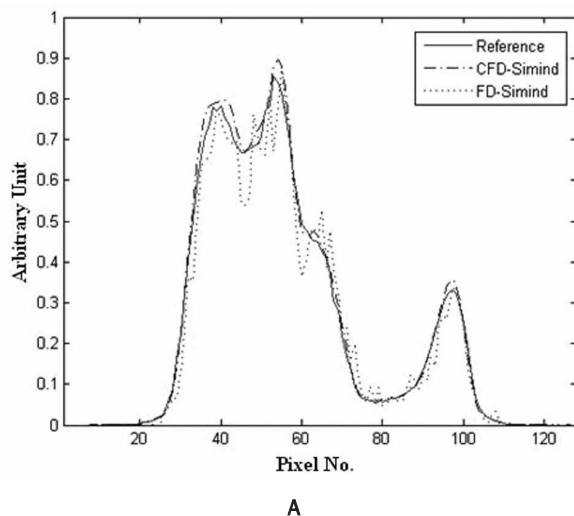
Figure 5. Simulated projections of Zubal Phantom for 8×10^7 photon histories. Top row is reference projection based on 2×10^9 photon histories. The below row, B): CFD projection C): FD projection.

generated with FD. This is confirmed by the profiles through the images of extended source projections (figure 6).

Estimated projections generated by CFD are much smoother, and are closer to the reference projection than those generated by FD for equal numbers of photon histories.

Figure 6 illustrates the line profiles of projections shown in reference image (figure 5) A, horizontal line profile; B, vertical line profile. There is good correlation between reference and CFD projection for 8×10^7 photon histories while there is more fluctuation in profiles for FD projection. But

the line profiles are almost the same as CFD method (with 8×10^7) when using 4×10^8 photon histories for FD method.

Figure 7 shows the UIQI (Q factor) as a function of the number of photon histories for CFD and FD. For equal numbers of photon histories, CFD produces projections which have a Q factor which is higher than that for FD.

It has been shown the speed up factor for CFD-SIMIND relative to FD-SIMIND as a function of UIQI and number of generated photon histories, is from 10 to 80 times more than FD in the same UIQI value [7].

Figure 7. UIQI (Q) values as a function of photon history for FD method (dashed line) and CFD method (solid line).
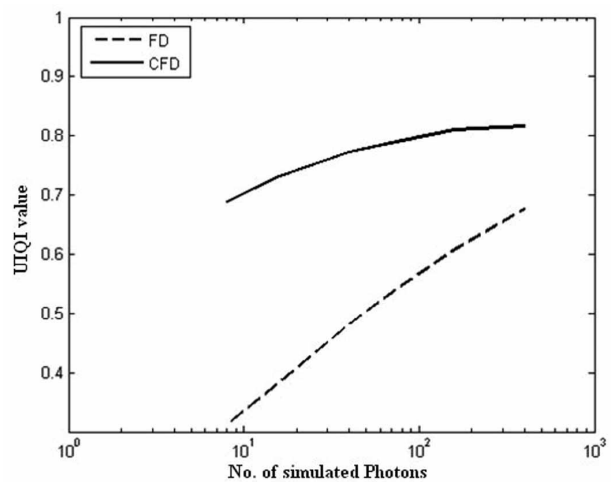

Figure 6. line profiles of different projections. A) Horizontal line profile. B) Vertical line profile for Reference (solid line), FD method (dotted line) and CFD method (dashed line).

DISCUSSION

One of the most important features of MC technique is its ability to compensate image degradation effects such as scatter, attenuation and collimator response (including system spatial resolution and septal penetration) to detect lesion and activity quantification in a planar or SPECT study, specially when using medium and high energy photons like I^{131} for quantitative estimation of activity in radionuclide therapy.

The results of both the standard FD and CFD in this study, using point and extended sources in the uniform and non-uniform phantoms, (Zubal), have shown similar results, bearing in mind that for the same degree of accuracy the CFD technique is faster than FD.

Matching measured and Simulated PSF of camera system is a good criterion for validation of CFD code. Although the CFD is based on spatial averaging over point source position due to convolution process, it doesn't include the effects of hole patterns. However, for the distances to the collimator and pixel size used in the planar or SPECT acquisitions in nuclear medicine, these effects, are of minor importance on the CFD results.

To implement MC technique in routine clinical use, it should be accurate enough and as fast as possible. The best way to compensate for image degradation factors is through the accurate modeling of these effects in an iterative reconstruction algorithm [7, 8, 16]. Recently, efficient modeling of collimator and crystal scattering, and the images of lead X-rays produced in the collimator have also been developed [7-15, 17]. However, radionuclides such as I^{131} further complicate such modeling due to the moderate-to-high energies of photons they emit. I^{131} emits 364 keV photons with an abundance of 0.81 and additional photons with different abundances that all of them were implemented to isotope routine in CFD code.

In case of penetration, photon paths often deviate more from the path parallel to the collimator hole axis as compared to the situation described for simple distance-dependent camera response, which included collimator blurring and intrinsic camera resolution. Therefore in this case, the blurring kernel was modified by using the new collimator subroutine that had been implemented to SIMIND program. The inclusion of these features, however, makes simulation significantly slower. Thus, the problem is to perform the calculations fast enough to be applied practically in iterative reconstruction.

The simulated scatter projections should be converged as fast as possible, if MC is to be used for model-based iterative reconstruction. The CFD generated projections is based on 10^7 photon histories which correspond fairly well to the reference projection (figure 5). The speed up factor by using CFD is more than 10 times.

For many years, our department has been doing targeted radiotherapy without using planar or SPECT images as an estimation of activity in the organs and this work is the first step toward using MC as a tool to compensate image degradation effects in nuclear medicine images for quantitative application in radionuclide therapy.

CONCLUSION

CFD as a practical method for accelerating MC simulation in planar and SPECT imaging has been modeled and developed into the SIMIND MC program for accurate photon distribution estimates. Accuracy of this simulation method was evaluated using the point spread function measurement has been compared to conventional FD-MC and validated with experimental results acquired from a GE Infinia and ADAC EPIC Argus gamma camera. When using the CFD method, simulation times have been cut by a factor of at least 10 compared to standard variance reduction techniques.

ACKNOWLEDGEMENT

REFERENCES

1. Ljungberg M and Strand SE (1989) A Monte Carlo program for the simulation of scintillation camera characteristics. *Comp Prog Biomed,* **29***: 257-272.*
2. Harrison R (2006) SimSET. http://depts.washington.edu/~simset/html/simset_home.html.
3. Strulab D, Santinac G, Lazaroad D, Bretonad V, Morelab C (2003) GATE (Geant4 Application for Tomographic Emission): a PET/SPECT general-purpose simulation platform. *Nuclear Physics, B (Proc. Suppl.),* **125***: 75-79.*
4. Haynor DR, Harrison RL, Lewellen TK (1991) The use of importance sampling techniques to improve the efficiency of photon tracking in emission tomography simulations. *Med Phys,* **18***: 990-1001.*
5. Beck JW, Jaszczak RJ, Coleman RE, Sterner CF, Nolte P (1982) Analysis of SPECT including scatter and attenuation using sophisticated Monte Carlo modeling methods. IEEE Trans. *Nucl Sci,* **29***: 506-511.*
6. Ljungberg M and Strand SE (1991) Attenuation and scatter correction in SPECT for sources in a nonhomogeneous object: A Monte Carlo study. *J Nucl Med,* **32***: 1278-1284.*
7. de Jong HWAM, Slijpen ETP, Beekman FJ (2001) Acceleration of Monte Carlo SPECT simulation using convolution-based forced detection. *IEEE Trans Nucl Sci,* **48***: 58-64.*
8. Farncombe TH, Liu S King MA, Brill AB, Stabin MG (2006) Accelerated SPECT Monte Carlo simulation using convolution-based forced detection. San-Diego 53rd Society of Nuclear Medicine Annual Meeting.
9. Ljungberg M, Larsson A, Johansson L (2005) A new collimator simulation in SIMIND based on the delta-scattering technique. *IEEE Trans Nucl Sci,* **52***: 1370-1375.*
10. Zubal IG, Harrell CR, Smith EO, Rattner Z, Gindi G, Hoffer PB (1994) Two dedicated software, voxel-based, anthropomorphic (torso and head) phantoms. *Med Phys,* **21***: 299-302.*
11. Dewaraja YK, Ljungberg M, Koral KF (2000) Charactrization of scatter and penetration using Monte Carlo simulation in I -131 Imaging. *J Nucl Med,* **41***: 123-130.*
12. Wang Z and Bovik AC (2002) A universal image quality index. *IEEE signal processing letters,* **9***: 81-84.*
13. Autret D, Bitar A, Ferrer L, Lisbona A, Bardiès M (2005) Monte Carlo modeling of gamma cameras for I-131 imaging in targeted radiotherapy. *CANCER BIOTH Radio,* **20***: 77-84.*
14. Formiconi AR (2002) Collimators. *Q J Nucl Med,* **46***: 8.*
15. Beekman FJ, de Jong HWAM, van Geloven S (2002) Efficient fully 3D Monte Carlo based statistical SPECT reconstruction. *IEEE Trans Med Imaging,* **21***: 867-77.*
16. Liu S, Khosravi HR, Farncombe TH (2006) Spect image reconstruction using convolution based forced detection monte carlo study. 5th annual symposium of imaging network, Ontario, Toronto, Canada.
17. de Jong HWAM, Wang WT, Frey EC, Viergever MA, Beekman FJ (2002) Efficient simulation of SPECT down-scatter including photon interactions with crystal and lead. *Med Phys,* **29***: 550-560.*